Measurement report: Formation of tropospheric brown carbon in a lifting air mass

Can Wu[1,2], Xiaodi Liu[1], Ke Zhang[1], Si Zhang[1]*, Cong Cao[3,4], Jianjun Li[3], Rui Li[1,2], Fan Zhang[1,2], Gehui Wang[1,2]*

[1]Key Lab of Geographic Information Science of the Ministry of Education, School of Geographic Sciences, East China Normal University, Shanghai 210062, China
[2]Institute of Eco-Chongming, 20 Cuiniao Rd., Chongming, Shanghai 202150, China
[3]State Key Laboratory of Loess and Quaternary Geology, Institute of Earth Environment, Chinese Academy of Sciences, Xi'an 710061, China
[4]School of Marine and Atmospheric Science, Stony Brook University, Stony Brook, NY 11794, USA

*Corresponding authors: Dr. Si Zhang, E-mail: szhang@geo.ecnu.edu.cn
Prof. Gehui Wang, E-mail: ghwang@geo.ecnu.edu.cn

30 **Abstract:** An enhanced formation of brown carbon (BrC) with a non-negligible warming effect

31 at the tropopause has recently been found. However, its formation mechanism is unclear. Here

32 we report a BrC formation process that happens during air mass upward transport by

33 conducting simultaneously a 4-hour time resolution of measurement on atmospheric BrC at the

34 mountain foot (MF, 400m a.s.l.) and mountainside (MS, 1120m a.s.l.) of Mt. Hua, China in

35 2016 summer. Our results showed that the daytime light-absorption (Abs_{365nm}) of BrC at MS is

36 approximately 60% lower than that at MF due to a dilution effect caused by the planetary

37 boundary layer expansion, but the daytime light-absorption of BrC relative to black carbon at

38 MS is about 30% higher than that at MF, suggesting a significant formation of secondary BrC

39 in the lifting process of air mass from MF to MS. Such a secondary formation accounted

40 for >50% of BrC at MS but only 27% of BrC at MF. Moreover, N:C elemental ratio of the

41 daytime BrC was 15% higher at MS than that at MF, mainly due to an aerosol aqueous phase

42 formation of water-soluble organic nitrogen (WSON) compounds. Stable nitrogen isotope

43 composition further indicated that such light-absorbing WSON compounds were produced

44 from the aerosol aqueous-phase reaction of carbonyls with NH_4^+. Our work for the first time

45 revealed that ammonia -induced aerosol aqueous reactions can significantly promote BrC

46 formation during the air mass lifting process, which is probably responsible for an enhanced

47 light absorption of BrC in the upper boundary layer.

48 **Keywords:** Brown carbon; Ammonia and carbonyls; Nitrogen-containing organic compounds;

49 Air mass upward transport; Aerosol aqueous-phase reaction.

50

1. Introduction

Light-absorbing organic aerosols, known as brown carbon (BrC), can efficiently absorb solar radiation in the visible to near ultraviolet (UV) wavelength range (Laskin et al., 2015; Liu et al., 2020a; Chakrabarty et al., 2023a) which is corresponding to 27~70% of black carbon (BC) light-absorption in the lower troposphere (Saleh et al., 2015; Lin et al., 2014; Lin et al., 2015) suggesting that BrC can perturb substantially the planetary radiation budget (Qian et al., 2015; Lin et al., 2014; Liu et al., 2015). By absorbing solar radiation at short wavelengths, BrC can strongly alter local gas-phase photochemistry and atmospheric oxidation through decreasing the photolysis rates of OH radicals, NO_2 and O_3, leading to a reduction in atmospheric oxidant concentration by up to ~30% (Hammer et al., 2016; Gligorovski et al., 2015; Jo et al., 2016). BrC in the atmosphere also acts as photosensitizers and produces active intermediates, and thus can promote sulfate formation (Liu et al., 2020b). In addition, BrC comprises numerous organic species and can induce adverse human health effects, because some of chromophores are toxic (Huang et al., 2018; Hsu et al., 2014; Yan et al., 2018).

Atmospheric BrC has both primary and secondary sources. Biomass burning is believed to be the major source of primary BrC (Chakrabarty et al., 2023b), while emissions from fossil fuel combustion is also an important source of primary BrC in the urban atmosphere (Yan et al., 2017; Corbin et al., 2019), which accounts for even more than 40% of the total BrC in heating season (Li et al., 2023). In the past decades numerous studies reported that BrC can also be secondarily generated in the atmosphere, such as photooxidation of aromatics under high NOx conditions (Lin et al., 2015; Liu et al., 2021), NH_4^+-initiated reactions with atmospherically relevant carbonyls (Li et al., 2021b; Kampf et al., 2012; Laskin et al., 2014; Li et al., 2019b)

73 and $\cdot OH/NO_3 \cdot$ radical oxidations of various VOCs (Sumlin et al., 2017; Gelencser et al., 2003;

74 Lu et al., 2011). BrC is chemically active, which may undergo photobleaching (Schnitzler et al.,

75 2022; Gilardoni et al., 2016), posing significant challenges for characterizing BrC molecular

76 composition and its links to optical properties.

77   Recently a aircraft measurement conduced over the continental United States observed an

78 enhanced short-wavelength optical absorption of BrC relative to BC at altitudes between 5 and

79 12 km (Zhang et al., 2017), indicating that secondary formation is one of crucial sources for

80 these high-altitude BrC. Numerical model studies reported that global radiative forcing caused

81 by BrC ranges from 0.1-0.6 Wm^{-2} (Zhang et al., 2020; Lin et al., 2014; Druge et al., 2022),

82 suggesting a non-negligible impact of BrC on the global climate change. Studies found that

83 such climate effects are highly sensitive to BrC and the sensitivity rapidly increases along with

84 an increase in altitude (Zhang et al., 2017; Nazarenko et al., 2017; Hodnebrog et al., 2014).

85 These abundant BrC at the tropopause would bring about prominent impacts on radiative

86 forcing, which is even twice of that induced by low-altitude BrC (Zhang et al., 2017). Due to

87 the limited number of field observations, however, the vertical distribution and formation

88 mechanism of tropospheric BrC are still unclear especially those in the upper troposphere,

89 where the direct radiative forcing of BrC is much stronger than that in the ground surface

90 atmosphere.

91   To elucidate the formation mechanism of BrC in the troposphere, synchronous

92 observations on atmospheric BrC were conducted on the mountainside and the mountain foot

93 of Mt. Hua, which is located closely to Guanzhong Basin, one of the areas with heaviest $PM_{2.5}$

94 pollution in China owing to intensive activities of fossil fuel combustion and the unfavorable

topography (Wang et al., 2022b; Wu et al., 2020; Wang et al., 2011; Wang et al., 2016). Our previous study has shown that inorganic aerosol chemistry in the atmosphere over Mt. Hua is dominated by the air mass transport from the Guanzhong Basin ground surface, in which $(NH_4)_2SO_4$ is continuously produced during the air mass lifting process along with a decrease in aerosol acidity (Wu et al., 2022). Here, we investigated the formation mechanism of secondary BrC during the lifting process of air mass from the Guanzhong Basin to the mountainous atmosphere of Mt. Hua. We firstly discussed the differences in vertical distribution and optical absorption of water-soluble BrC between the ground surface and the mountainous atmosphere, then explored their formation mechanism in the upper boundary layer. To the best of our knowledge, we for the first time found that ammonia-induced aerosol aqueous phase reaction with carbonyls is the dominant formation pathway of BrC in the air mass lifting process, which is responsible for the high ratio of BrC to BC in the top troposphere.

2. Materials and Methods

2.1 Sample Collection

Offline $PM_{2.5}$ samples with a 4-hour interval were synchronously collected onto prebaked quartz filters (at 450 °C for 6 h) at two locations of Mt. Hua from 27 August to 17 September 2016. One sampling site locates at the mountain foot (MF, 34°32′N, 110°5′E; 400 m a.s.l.) and another one is situated on the mountainside (MS; 34°29′N, 110°3′E; 1120 m a.s.l.) with little anthropogenic activities due to its steep terrain in the mountain region. The horizontal distance between the two sites is ~8 km and the vertical distance is about 1km (Figure S1). As revealed in our previous study (Wu et al., 2022), vertical divergence simulated by WRF-Chem model

decreased gradually as enhanced elevation, along with the prevailing southerly winds, indicating

a feasibility of vertical transport of air parcel from MF to MS. And we also note that the change

of emission sources among two site was insignificant in a lifting air mass as indicated by

indistinctive divergences of diagnostic ratios and proportion of organic tracers from emission

sources. Such conditions can avoid the interferences caused by the emission sources change when

exploring aging process of BrC. More descriptions on the two sites have been documented by

our previous study along with the details on the sampling instrument setup (Wu et al., 2022).

Mass concentrations of $PM_{2.5}$, NO_2 and O_3 at MS site were directly quantified by E-BAM (Met

One Instruments, USA) and NOx and O_3 Analyzer (Thermo, Model 42i, USA; Thermo, Model

49i, USA), respectively. At MF site, the data of above species apart from $PM_{2.5}$ monitored by

another E-BAM were downloaded from the Weinan Ecological Environment Bureau

(http://sthjj.weinan.gov.cn/, last access: 8 July 2021). Meteorological parameters of both

sampling sites were downloaded from the Shaanxi Meteorological Bureau website

(http://sn.cma.gov.cn/, last access: 8 July 2021).

2.2 Chemical Analysis

The organic carbon (OC) and element carbon (EC) of $PM_{2.5}$ filter samples were quantified

by a DRI model 2001 thermal–optical carbon analyzer following the IMPROVE-A temperature

protocol (Chow et al., 2007). Water-soluble organic carbon (WSOC) and water-soluble total

nitrogen (WSTN) of $PM_{2.5}$ were extracted using Milli-Q pure water (18.2 MΩ) and determined

using a total organic carbon (TOC) analyzer (Model TOC-L CPH, Shimadzu, Japan). Water-

soluble organic nitrogen (WSON) is calculated by deducting the water-soluble inorganic

nitrogen (WSIN) from WSTN (i.e., WSON=WSTN-WSIN). Molecular compositions (e.g.,

139 nitrophenols, PAHs and other organic tracers) in the $PM_{2.5}$ filter samples were quantified by a

140 gas chromatography (HP 7890A, Agilent Co., USA) coupled with mass spectroscopy detector

141 (GC/MS) (HP 5975, Agilent Co., USA) after the sample extraction and derivatization. Th

142 details of the extraction and derivatization can be found elsewhere (Li et al., 2023; Li et al.,

143 2020; Wang et al., 2006). Briefly, one-fourth of the filter sample was extracted with a mixture

144 of methanol and dichloromethane (2:1, v/v). Then the extracts were derivatized with N,O-bis-

145 (trimethylsilyl) trifluoroacetamide (BSTFA).

146   The stable nitrogen isotope compositions of NH_4^+ ($\delta^{15}N\text{-}NH_4^+$) were determined by the

147 isotopic analysis of nitrous oxide (N_2O) derived from chemical conversion of NH_4^+, and finally

148 quantified by a Precon-GasBench-IRMS system. This is a reliable method for nitrogen isotope

149 analysis of the sample with low NH_4^+ concentration, of which precision can be up to 0.2‰.

150 More details upon the analytical artifact and quality control protocols can be found in our

151 previous studies. Furthermore, only the daytime samples were analyzed for the $\delta^{15}N\text{-}NH_4^+$ here,

152 and a merging pretreatment was applied for the daily samples to meet for the analysis

153 requirements.

154   Additionally, a high-resolution time-of-flight aerosol mass spectrometer (Aerodyne

155 Research Inc., Billerica, MA, USA) was employed to determine the chemical compositions of

156 water-soluble organic matter (WSOM) in $PM_{2.5}$, of which the method is similar to the report by

157 Daellenbach et al. (2016). The offline analytical procedure has been reported previously, here

158 we only give a brief description (Ge et al., 2017; Sun et al., 2011). One-eighth of the $PM_{2.5}$

159 filter samples was extracted with pure water. Then, the water-extracts were atomized using

160 argon as carrier gas, dried by a diffusion drier, and ultimately quantified by the aerosol mass

161 spectrometer. Purified water was also treated in the same manner prior to each sample running,

162 which was deemed as an analytical blank. As we mainly focused on the WSOM chemical

163 composition, a deep post-processing was conducted for the V-mode data in this study using the

164 Igor-based Aerosol Mass Spectrometer Analysis Toolkit. Element ratios of WSOM including

165 oxygen-to-carbon (O/C), hydrogen-to-carbon (H/C), nitrogen-to-carbon (N/C) , and organic

166 mass-to-organic carbon (OM/OC) ratios were determined according to the Improved Aiken (I-

167 A) method (Canagaratna et al., 2015). The mass load of WSOM in ambient air can be

168 accurately estimated using Eq.1, since the chemical species concentration in atomized aerosols

169 depends on the flow rate of the carrier gas and extract concentration.

$$WSOM = WSOC \times OM/OC_{WSOM} \qquad \text{Eq. 1}$$

170 Where WSOM is water-soluble organic matter (WSOM) in the atmosphere ($\mu g\ m^{-3}$),

171 WSOC is water-soluble organic carbon (WSOC, μgCm^{-3}) in the atmosphere and measured by

172 the TOC analyzer, and OM/OC$_{WSOM}$ is the mass ratio of WSOM and OC determined by the

173 aerosol mass spectrometer. To obtain reliable data, the ionization efficiencies of HR-AMS was

174 calibrated with 300 nm (D_m) ammonium nitrate and ammonium sulfate particle following the

175 standard protocols (Sun et al., 2020; Jayne et al., 2000); and the relative ionization efficiencies

176 (RIEs) of 4.1 and 0.8 were used for ammonium and sulfate. While, the default RIEs were

177 applied for organics, nitrate and chloride.

178 **2.3 Optical Absorption of BrC**

179   Measurement of UV−vis absorption spectra of water-soluble BrC in PM$_{2.5}$ was performed

180 using a liquid waveguide capillary UV−vis spectrometer with a long effective path length (1

181 m). The extracted solution of BrC were prepared by a similar treatment to WSOC (Text S1), of

which absorption spectra were converted into the absorption coefficient at a given wavelength λ

(abs$_\lambda$, M/m, eq S1). The mass absorption efficiency (MAE$_\lambda$, m^2/gC) corresponding to water-

soluble BrC at a given wavelength λ can be calculated as follows:

$$MAE_\lambda = \frac{abs_\lambda}{M} \qquad \qquad \text{Eq. 2}$$

Where M (μgC/m^3) is the mass concentration for water-soluble organic carbon (WSOC).

Absorption Ångström exponent (AAE) indicates the spectral dependence of a species, which

was quantified by a linear regression of log (abs$_\lambda$) versus log (λ) over a wavelength rang of 300-

500 nm (Wu et al., 2020).

2.4 Positive matrix factorization (PMF) source apportionment

To quantitatively determine the fractional contribution of specific sources to BrC, a PMF

receptor model (EPA PMF 5.0 version) coupled with a bootstrap technique was applied here, of

which principle has been documented in previous studies (Brinkman et al., 2006; Paatero and

Tapper, 1994). Briefly, WSOC, WSON, SO$_4^{2-}$, NH$_4^+$, Mg^{2+}, Ca^{2+}, abs$_{365\ nm}$ and organic tracers

(BbF, Bghip and levo.) are the input variables in the present work, all of which are regarded as

strong variable expect for Bghip with a low S/N ratio (0.6). Another input dataset is uncertainty

matrix that is calculated according to the following equations (Eq.3). The uncertainties of each

factor profile are also evaluated by a bootstrap analysis, of which result showed that

reproducibility of each source factor was >80% (Table S1), indicating a well robustness. In our

previous study on Mt. Hua (Wu et al., 2022), insignificant change in the corresponding emission

sources was revealed during air mass lifting process. Thus, the daytime samples from both sites

were added together as one data matrix. Considering Q values and interpretability, four factors

were obtained as the optimal solution after numerous testes with three to seven factors, and the

203 input species matched well with simulated ones with significant correlations ($R^2 > 0.88$).

$$\text{uncertainty} = \begin{cases} \dfrac{5}{6} \times \text{MDL} & (\text{concentration} < \text{MDL}) \\ \sqrt{(\text{error fraction} \times \text{concentration})^2 + (0.5 \times \text{MDL})^2} & (\text{concentration} > \text{MDL}) \end{cases} \quad \text{Eq.3}$$

204 Where MDL is the method detection limit. And the error fraction is set to 5% for $PM_{2.5}$ (Gao

205 et al., 2018); WSOC, WSON, SO_4^{2-}, NH_4^+, Mg^{2+}, Ca^{2+} are estimated to be 7 %, those of other

206 species are 12%. To reduce the error, the sample with missing data for individual species would

207 be excluded rather than replace by the mean value of whole campaign.

208 **2.5 Random forest analysis for WSON**

209 Random forest (RF), as a powerful tool, has been used widely in the regression and prediction

210 problems upon atmospheric pollutions, even the data have complex nonlinear relationships and

211 interactions (Hu et al., 2017; Vu et al., 2019). To reveal the key factors that may affect the WSON

212 formation during the air mass lifting process, a RF regression model was applied for the daytime

213 samples at MF and MS sites, respectively. And the potential factors, including pH, ALWC, T, RH,

214 NH_4^+, NH_3(aq), NO_2, nitrophenols, O_3 and organic matter (OM), herein were regarded as the

215 predictors for WSON. In the RF model design, about 70% of these original data were randomly

216 divided into the training dataset to construct the RF model, and the rest was deemed as the testing

217 data for testing the model performance. There are two important parameters being constantly

218 optimized in the model construction process, including the number of trees grown (n_{tree}) and

219 number of variables split at each node (n_{mtry}); After numerous tests, n_{tree} and n_{mtry} were set as 100

220 and 10 for MF data, and 128 and 9 for MS data, respectively, to achieve the best prediction

221 accuracy. Furthermore, a 10-fold cross-validation technique was employed here to

222 simultaneously tune model parameters and estimate model performance. And the statistical

223 metrics including coefficient of determination (R^2), mean square error (MSE) or root-mean-

224   square error (RMSE) and mean absolute error (MAE), were established to evaluate prediction

225   accuracy of the model. As shown in Table S2, the predicted data for the testing dataset has strong

226   correlativity with observed ones, with small values for those error metrics; These results indicated

227   a satisfactory performance of the RF model for explain the importance of these factors to daytime

228   WSON formation.

3. Results and Discussion

3.1 Enhanced Light Absorption of BrC in the Mountainous Atmosphere

231   Figure 1 shows the temporal variations in light absorption (abs_{365nm}) and concentrations of

232   fine particulate WSOC simultaneously observed at the mountain foot (MF) and mountainside

233   (MS) sites. The variation patterns of water-soluble BrC (i.e., $abs_{365\,nm}$) at both sites were closed

234   followed by WSOC ($R^2 > 0.70$, Figure 1 and Figure S2); this indicated that BrC is an important

235   part of WSOC, of which light absorption of BrC markedly increased with a decrease in light

236   wavelengths. As summarized in Table 1, the averaged $abs_{365\,nm}$ of BrC was 2.1 ± 1.4 M m^{-1} at

237   MS, approximately corresponding to 40% of that (5.1 ± 2.4 M m^{-1}) at MF. The light-absorbance

238   level of BrC at the high altitude MS site is in the same range as those reported from Chinese

239   megacities such as Beijing (Cheng et al., 2016) and Xi'an (Wu et al., 2020), indicating a strong

240   light-absorption of BrC in the upper boundary layer over Guanzhong Basin, inland China.

241   Absorption Ångström exponent (AAE) at MS is 5.7 ± 1.3 (Table 1), slightly lower than that at

242   the ground MF site (6.0 ± 0.5). Such a difference in AAE ($p < 0.05$) is most likely related to the

243   difference in chemical composition of the chromophores between the two sites with different

244   altitudes. The averaged mass absorption efficiency (MAE) at MS ($MAE_{365\,nm}$, 0.67 ± 0.2 m^2 g^{-1})

245   was almost equal to that at MF (0.69 ± 0.2 m^2 g^{-1}) but 30-40% higher than those observed in

246 Chinese megacities such as Beijing (Du et al., 2014) and Nanjing (Chen et al., 2018) (~0.5 m^2

247 g^{-1}, in summertime), further demonstrating a strong light-absorption nature of BrC in the upper

248 boundary layer of Guanzhong Basin, inland China.

249   Figure 2 shows the diurnal variations of $abs_{365\ nm}$ and $MAE_{365\ nm}$ at both sites during the

250 campaign. At MF site a morning peak of $abs_{365\ nm}$ driven by enhanced traffic emissions

251 occurred at 8:00~12:00 (local time, thereinafter), and then gradually decreased and reached a

252 minimum at 12:00~16:00 with the lowest MAE at 365 nm wavelength ($MAE_{365\ nm}$, 0.57±0.14

253 $m^2\ g^{-1}$ (Figures 2a and 2b). Such a ground surface decease in light absorption of BrC at early

254 afternoon can be attributed to the daytime boundary layer growth and photobleaching. This can

255 be verified by the oxidation state of carbon (OSc) measured by the aerosol mass spectrometer,

256 of which higher value is indicative of a deeper degree of atmospheric oxidation (Li et al.,

257 2019a). As seen in Figure 3a, $abs_{365\ nm}$ negatively correlated with OSc, which is consistent with

258 those reported by previous laboratory experiments (Lee et al., 2014; Zhao et al., 2015; Sumlin

259 et al., 2017) and suggests that atmospheric aging can significantly diminish the light-absorption

260 of BrC. On the contrary, abs_{365nm} at MS site remarkably enhanced with the boundary layer

261 growth and peaked at 12:00~16:00 (Figure 2a), despite the fact that the aerosol was further

262 oxidized during the upward transport as indicated by the a higher OSc value at MS site (Figure

263 3b); The OSc variation among both sites coincided with that of BaP/BeP being a known proxy

264 of whether aerosols are freshly emitted (> 1) or aged (< 1) (Figure S3). Moreover, a moderate-

265 increased MAE_{365nm} was also observed in this process (Figure 2b). As shown in Table 1, the

266 light absorption of BrC at 365 nm relative to BC at 550 nm (abs_{365}-BrC/abs_{550}-BC) during the

267 daytime at MS was 0.28±0.08, which is approximately 30% higher than that (0.22±0.08, Table

1) at MF. Our previous study at Mt. Hua found that changes in sources of primary organic aerosols in the air mass transported from MF to MS were insignificant (Wu et al., 2022), indicating that there was no additional emission of BrC during the air mass upward transport. Thus, the enhanced light-absorption of BrC relative to BC at MS is solely ascribed to a secondary formation of absorbing BrC (Figure 2c); and these secondary BrC were highly light-absorbing despite more aged atmosphere aloft, as verified by a strongly positive correlation between MAE_{365nm} and OSc values at MS site (Figure S4).

To further elucidate the above hypothesis, a PMF analysis was applied for the source apportionment of the daytime $abs_{365\ nm}$ at both sites. As seen in Figure S5, four types of BrC sources were identified. In brief, fossil fuel combustion and biomass burning influenced by local-related emissions were primary sources for the surface BrC, consistent with observations in other cities (Li et al., 2023; Wu et al., 2020; Wang et al., 2022a). However, BrC at MS site was produced dominantly from secondary formation, of which the contribution to the total BrC is 53% and about twice of that at MF (Figure 2d) further corroborating a substantial formation of BrC with relatively stronger light-absorptivity during the air mass lifting process. These secondarily formed BrC chromophores engender a more light-absorption of high-altitude BrC compared with that of BC (or EC, Figure 2c); Similar vertical profile of BrC in the upper troposphere (5~12 km) of the continental US was also observed by in-situ aircraft measurements (Zhang et al., 2017).

3.2 Secondary Formation of BrC in the Air Mass Lifting Process

Figure 4a illustrates the diurnal cycles of N:C ratio of the water-soluble organic matter in $PM_{2.5}$ measured by the high-resolution time-of-flight aerosol mass spectrometer. At the MF site

290   N:C ratio did not vary much with time and was even leveling off in the daytime, which

291   indicates that the compositions of light-absorbing chromophores are similar throughout the day.

292   Nonetheless, the diurnal pattern of N:C ratio at MS was analogous to that of $abs_{365\ nm}$ and

293   $MAE_{365\ nm}$ with a daily peak at 12:00~16:00 and a moderate positive correlation was also

294   observed between N:C ratio and $abs_{365\ nm}$ (R^2=0.38, P<0.01), suggesting that nitrogen-

295   containing organic compounds (NOCs) have significant contributions to the BrC light-

296   absorption in the upper boundary layer. Such a results is consistent with the laboratory

297   simulation, in which NOCs have been reported to contribute up to 60% of the absorbance of

298   secondary BrC over a wavelength rang of 300−400 nm (Lin et al., 2015). Moreover, the

299   daytime N:C ratios were 20% higher at MS (0.066±0.014) than those at MF (Figure 4a),

300   indicating that additional NOCs were produced in the air mas lifting process. In fact, numerous

301   N-containing organic fragments including C_xH_yN and $C_xH_yO_zN$ at the MS site were detected by

302   the aerosol mass spectrometer, accounting for ~13% of the total water-soluble OM; And

303   fractional contribution of above fragments at MS enhanced by approximately 10% compared to

304   that at MF site, even up to ~25% at the day with low $PM_{2.5}$ load (<75 μg/m^3) (Figure S6). This

305   suggested an enhanced formation of WSON during the air mass transport from the lower

306   mountain foot site to the upper mountainside site. Since WSON at MS moderately was

307   positively correlated with light absorption of BrC at λ=365nm (Figure S7, R^2=0.45, p<0.05),

308   the enhancement in BrC light-absorption at MS can largely be attributed to secondary

309   formation of NOCs during the air mass transport from the ground surface to the upper

310   boundary layer.

311   Light-absorbing NOCs including reduced nitrogen species (e.g., imidazoles and pyrazines)

312 and oxidized ones (e.g., nitroaromatics) can be generated via various types of gas- and particle-

313 phase reactions, such as, NH_3-mediated carbonyl-to-imine reactions, nitration of aromatic

314 compounds, and heterogeneous reactions of ·OH and NO_2^-· radicals with phenolic compounds

315 (Moise et al., 2015; Laskin et al., 2015). The potential pathways and dominating factors for

316 NOCs formation at MS site will be explored in the following sections.

317 **3.3 Gas-Phase Formation of BrC in the Air Mass Lifting Process**

318 Nitroaromatic compounds (NACs) are strong light-absorbing compounds and are

319 ubiquitous in the atmosphere. In this study, a total of six NACs in the $PM_{2.5}$ samples were

320 detected (Table S3), which exhibited a significant correlation with $abs_{365\ nm}$ at both sampling

321 sites (Figure S2c and S2d), indicating an important impact of NACs on the aerosol light-

322 absorption. As seen in Figure 5a, both NACs concentration and NACs/OC ratio decreased

323 gradually at MF, reaching the daily minimum at 12:00-16:00. Such an abatement in NACs was

324 mainly attributed to the boundary layer expansion and an enhanced photooxidation (Figure 3).

325 Furthermore, the daytime NACs at MF well correlated with (BbF+levoglucosan) being known

326 as tracers for combustion emissions (R^2>0.76, Figure 5c), but not correlated with gaseous NO_2

327 (Figure 5e), suggesting that most of NACs at the ground surface site were directly emitted from

328 combustion sources. This can be further verified by a strong positive correlation of NACs and

329 CO prevailing in combustion exhausts (Figure S8). As partial NACs at the MF site can be

330 transported aloft by anabatic valley winds, thus a moderate correlation (R^2=0.49, Figure 5d)

331 between NACs and (BbF+levoglucosan) was observed at MS site. However, a moderate

332 correlation between NO_2 and NACs (R^2=0.57, p<0.01, Figure 5f) observed at MS suggests a

333 non-negligible formation of secondary NACs under the transport process. As revealed by

previous studies, the $NO_3 \cdot / \cdot OH$-oxidation of phenolic volatile organic in the presence of NOx

can form numerous NACs that followed by partitioning to the condensed phase (Wang and Li,

2021; Li et al., 2021a; Finewax et al., 2018); and the photolysis of nitrite in aerosol aqueous

phase can also lead to the nitration of phenol/catechol to generated NACs (Vione et al., 2005).

But a poor relationship between NACs and aerosol liquid water content (ALWC; R^2=0.34,

P>0.05) and particulate phenol (R^2<0.1), indicating a minor contribution of aqueous-phase

formation to NACs aloft.

The preceding discussion provided reliable evidences that partial NACs could be formed

by gas-phase reactions, but they only accounted for a very small fraction of OC (Figure 5a-b),

suggesting that gas-phase formation is probably not the major formation pathway of secondary

NOCs during the air mass vertical transport. Further evidence for this hypothesis was provided

by a random forest (RF) analysis being used as a metric for the degree of correlation between

these influencing factors (ALWC, pH, T, NO_2, NH_4^+, etc.) and WSON at both sampling sites

(Figure 4b and Figure S9). As revealed by RF model results, nitrophenols and gaseous NO_2

were important influencing factors for the daytime WSON at MF site (Figure S9), of which

importance was explained up to 35% but only~15% of that aloft (Figure 4b), confirming a less

importance of the gas-phase reactions for the light-absorbing NOCs formation in the vertical

transport process.

3.4 Aerosol Aqueous Formation of BrC in the Air Mass Lifting Process

As shown in Figure 4b, RF analysis showed that the variation in concentration of WSON

in $PM_{2.5}$ at MS was largely affected by NH_4^+ (23.0%) and ALWC (17.3%). Given a relatively

strong correlation between WSON and NH_4^+ (R^2=0.70, Figure 4c), we proposed that aqueous

356 phase reactions induced by ammonium is the major formation pathway for water-soluble NOCs

357 at MS. For further demonstrating such a hypothesis, we analyzed nitrogen isotope composition

358 ($\delta^{15}N$-NH_4^+) of ammonium in the $PM_{2.5}$ samples at both sites, of which the analytical details

359 has been described in our previous study (Wu et al., 2022). As seen in Figure 4d, WSON

360 showed a strong negative correlation with $\delta^{15}N$-NH_4^+, probably due to the irreversible reactions

361 involving ammonia favored ^{15}N depletion in the particle form as revealed by Heaton et al.

362 (1997). In contrast, WSON at MF presented a similar correlation with NH_4^+ as that at MS but

363 did not correlate with $\delta^{15}N$-NH_4^+ (Figures S10 (a) and (b)).

364   Previous studies have demonstrated the importance of NH_4^+/NH_3 in the formation of light-

365 absorbing imidazoles and N-heterocycles from the carbonyls (e.g., glyoxal (Gly) and

366 methylglyoxal (mGly) generated from oxidation of VOCs) (Li et al., 2021b; Moise et al., 2015;

367 Kampf et al., 2012; Liu et al., 2023). Figure S11 depicts a simple reaction pathway for above

368 aqueous reactions, in which the chromophore products contain less amounts of O and H atoms.

369 Such a phenomenon was found for the daytime NOCs at MS. As shown in Figure 6, the H/N

370 and O/N ratios of BrC in $PM_{2.5}$ at MS exhibited a strongly negative correlation with N/C ratio,

371 respectively ($R^2=0.92$ for H/N and $R^2=0.84$ for O/N). Considering the fact that Gly and mGly

372 are abundant at the daytime atmosphere of Mt. Hua (Qi et al., 2023), the aqueous reactions of

373 dicarbonyls with NH_4^+/NH_3 are probably the major pathway to yield NOCs during the vertical

374 transport.

375   Above aqueous reactions could also occur at MF site as depicted in Figure S11, but it was

376 insignificant compared to that at MS site, attributing the disparity in chemical compositions.

377 Our previous study found that the ground surface MF aerosols were more acidic (pH=2.9) and

378 dominated by NH_4HSO_4, while the upper boundary layer MS aerosols were less acidic

379 (pH=3.4) and dominated by abundant $(NH_4)_2SO_4$. Such differences in aerosol acidity and

380 chemical compositions between two sites can favor the formation of NOCs at the MS site, as

381 evident from a recent experimental observation by Li et al. (2021b), who found that NOCs

382 yield on the $(NH_4)_2SO_4$ seeds exposing to Gly or mGly vapor was relatively higher than that on

383 NH_4HSO_4 seeds. Also, they found that mGly has a larger uptake coefficient on $(NH_4)_2SO_4$

384 particles with a relatively higher NOCs yield compared to Gly, because mGly has a stronger

385 interfacial attraction and thus has a more efficient nucleophilic addition involving the

386 carbenium ions (Li et al., 2021b). Our previous study showed that the summertime atmosphere

387 of Mt. Hua is dominated by biogenic VOCs and the concentration of fine particulate mGly is

388 about five times that of Gly (Meng et al., 2014). Such a predominance of mGly over Gly and a

389 less acidic aerosol aqueous aerosol phase at the MF site are favorable for light-absorbing NOCs

390 formation on $(NH_4)_2SO_4$ particles, which can mainly be responsible for the enhanced light

391 absorption of BrC at the mountainous site with the ratio of light absorption of BrC to BC higher

392 in the upper boundary layer than that in the ground surface.

393 **3.5 Atmospheric implications**

394   Our work provides an evolution profile of BrC during air mass vertical transport, and

395 highlights a secondary formation of BrC in this process, which can be responsible for the

396 enhancement of BrC relative to BC in the upper boundary layer. As the longer lifetime of high-

397 altitude BrC, they can disperse rapidly into a large area (Zhang et al., 2017), exerting

398 significant influence on regional climate that is even comparable to BC in the upper tropical

399 troposphere (Jo et al., 2016). Moreover, we also revealed a vital role of aqueous-phase

reactions for the secondary formation of BrC in the air mass lifting process, specifically the

NH_4^+/NH_3-induced reactions (e.g., Maillard reaction) that can form NOCs with stronger light-

absorptivity. As ammonia and carbonyls such as glyoxal and methylglyoxal are ubiquitous in

the troposphere, thus our work suggests that the above formation mechanism on the light-

absorbing NOC aerosols could extensively occur in the troposphere.

In the past decade, the haze pollution in China has changed from previous sulfate-

dominated environment (SD) to the current nitrate-dominated environment (ND) due to the

effective sulfur emission control, which would significantly enhance the aerosol ALWC since

nitrate is more hygroscopic than sulfate at a given RH and aerosol loading. While, as indicated

by our previous observational evidences (Lv et al., 2023), high ALWC load induced by

abundant nitrate would efficiently promote more WSOC partitioning into the aerosol phase

compared with that in SD ones, and thus may increase the BrC yield because WSOC contains

numerous BrC precursors. With the increase in relative abundance of nitrate to sulfate, nitrate-

enhanced gas-to-particle partitioning of WSOC will become highly efficient in China in the

near future, meaning that the BrC formation will be more active hereafter. Additionally, the

national VOCs and NH_3 emissions have remained at high levels, and even have shown a slight

increasing trend. The abundant NH_3 can not only participates in the formation of BrC but also

affects BrC optical properties by regulating the aerosol acidity. To further reveal the impact on

the BrC, the NH_3 concentration and $MAE_{365\,nm}$ value of water-soluble BrC in different region

of China were statistically explored on a national scale (Figure 7a). As depicted in Figure 7a,

the spatial pattern of $MAE_{365\,nm}$ is closely coincident with NH_3 levels with a robust positive

correlation (R^2=0.87). Such a spatial distribution pattern indicates that NH_3-rich conditions are

favorable for formation of BrC with strong light-absorptivity. China is one of the countries with

strongest NH_3 emissions in the world due to huge demand for N-fertilizer (Van Damme et al.,

2018), and thus atmospheric NH_3 in China is much higher than that in Europe and the United

States. This is probably one of the factors causing the higher concentrations of BrC with

stronger light-absorptivity in China compared with developed countries (Figure 7b).

4. Conclusion

Synchronous observations upon optical properties and chemical compositions of

atmospheric BrC were conducted at MF and MS of Mt. Hua, and revealed that light-absorption

of BrC aloft was only ~40% of that at surface owing to a dilution effect caused by planetary

boundary layer upliftment. And the light-absorption of BrC relative to black carbon moderately

enhanced in the lifting process of air mass from MF to MS coincide with the variation of the

daytime MAE_{365nm} aloft, indicating a secondary formation of BrC; and these secondary BrC

accounted for >50% of total at MS site. While, the surface BrC was mainly originated from

direct combustion emission, with a 55% of fractional contribution to the total.

The N:C ratio of WSOM was measured by offline AMS, of which diurnal pattern was

analogous to that of $abs_{365\ nm}$ and $MAE_{365\ nm}$ aloft, substantiating a considerable contribution of

nitrogen-containing organic compounds (NOCs) to BrC light-absorption. And daytime N:C

ratio site was approximately 15% higher at MS than that at MF, mainly due to a significant

formation of secondary NOCs produced by NH_4^+/NH_3-induced reactions (e.g., Maillard

reaction). Moreover, a robust positive relationship between $MAE_{365\ nm}$ and NH_3 load was

statistically explored in nationwide, strongly manifested that abundant NH_3 maybe one of key

factors for the high BrC load with strong light-absorptivity in China compared to that in

444   developed countries. Therefore, NH_3 emission control in China is indispensable for further

445   alleviating haze and BrC pollutions in the country.

446   **Data availability.** The data used in this study are freely available at

447   https://doi.org/10.5281/zenodo.10926469 (Wu, 2024). And Meteorological data and hourly

448    $PM_{2.5}$, NO_2, O_3 concentrations can be obtained from https://doi.org/10.5281/zenodo.7413640

449   (Wu, 2022a).

450   **Author contributions.** G.W. designed research and contributed analytic tools. C.W., C.C. and

451   J.L. collected the samples. C.W., X.L., K.Z. and G.W. conducted the sample analysis. C.W.,

452   S.Z. and G.W. performed the data interpretation. C.W. and G.W. wrote the paper. All authors

453   contributed to the paper with useful scientific discussions.

454   **Competing interests.** The authors declare no competing interest.

455   **Acknowledgements.** This work was financially supported by the National Natural Science

456   Foundation of China (No. 42130704, 42007202) and ECNU Happiness Flower program.

457

458   **References**
459   Bosch, C., Andersson, A., Kirillova, E. N., Budhavant, K., Tiwari, S., Praveen, P. S., Russell, L. M., Beres, N. D.,
460   Ramanathan, V., and Gustafsson, O.: Source-diagnostic dual-isotope composition and optical properties of
461   water-soluble organic carbon and elemental carbon in the South Asian outflow intercepted over the Indian
462   Ocean, J. Geophys. Res.-Atmos., 119, 11743-11759, 10.1002/2014jd022127, 2014.
463   Brinkman, G., Vance, G., Hannigan, M. P., and Milford, J. B.: Use of synthetic data to evaluate positive matrix
464   factorization as a source apportionment tool for $PM_{2.5}$ exposure data, Environ. Sci. Technol., 40,
465   1892-1901, 10.1021/es051712y, 2006.
466   Canagaratna, M. R., Jimenez, J. L., Kroll, J. H., Chen, Q., Kessler, S. H., Massoli, P., Hildebrandt Ruiz, L., Fortner,
467   E., Williams, L. R., Wilson, K. R., Surratt, J. D., Donahue, N. M., Jayne, J. T., and Worsnop, D. R.: Elemental
468   ratio measurements of organic compounds using aerosol mass spectrometry: characterization, improved
469   calibration, and implications, Atmos. Chem. Phys., 15, 253-272, 10.5194/acp-15-253-2015, 2015.
470   Chakrabarty, R. K., Shetty, N. J., Thind, A. S., Beeler, P., Sumlin, B. J., Zhang, C., Liu, P., Idrobo, J. C., Adachi, K.,
471   Wagner, N. L., Schwarz, J. P., Ahern, A., Sedlacek, A. J., Lambe, A., Daube, C., Lyu, M., Liu, C., Herndon, S.,
472   Onasch, T. B., and Mishra, R.: Shortwave absorption by wildfire smoke dominated by dark brown carbon, Nat.
473   Geosci., 16, 683-+, 10.1038/s41561-023-01237-9, 2023a.
474   Chakrabarty, R. K., Shetty, N. J., Thind, A. S., Beeler, P., Sumlin, B. J., Zhang, C. C., Liu, P., Idrobo, J. C., Adachi,

K., Wagner, N. L., Schwarz, J. P., Ahern, A., Sedlacek, A. J., Lambe, A., Daube, C., Lyu, M., Liu, C., Herndon, S., Onasch, T. B., and Mishra, R.: Shortwave absorption by wildfire smoke dominated by dark brown carbon, Nature Geoscience, 16, 10.1038/s41561-023-01237-9, 2023b.

Chen, Y., Ge, X., Chen, H., Xie, X., Chen, Y., Wang, J., Ye, Z., Bao, M., Zhang, Y., and Chen, M.: Seasonal light absorption properties of water-soluble brown carbon in atmospheric fine particles in Nanjing, China, Atmos. Environ., 187, 230-240, 10.1016/j.atmosenv.2018.06.002, 2018.

Cheng, Y., He, K.-b., Du, Z.-y., Engling, G., Liu, J.-m., Ma, Y.-l., Zheng, M., and Weber, R. J.: The characteristics of brown carbon aerosol during winter in Beijing, Atmos. Environ., 127, 355-364, 10.1016/j.atmosenv.2015.12.035, 2016.

Chow, J. C., Watson, J. G., Chen, L. W. A., Chang, M. C. O., Robinson, N. F., Trimble, D., and Kohl, S.: The IMPROVE-A temperature protocol for thermal/optical carbon analysis: maintaining consistency with a long-term database, Journal of the Air & Waste Management Association, 57, 1014-1023, 10.3155/1047-3289.57.9.1014, 2007.

Corbin, J. C., Czech, H., Massabo, D., de Mongeot, F. B., Jakobi, G., Liu, F., Lobo, P., Mennucci, C., Mensah, A. A., Orasche, J., Pieber, S. M., Prevot, A. S. H., Stengel, B., Tay, L. L., Zanatta, M., Zimmermann, R., El Haddad, I., and Gysel, M.: Infrared-absorbing carbonaceous tar can dominate light absorption by marine-engine exhaust, npj Clim. Atmos. Sci., 2, 10.1038/s41612-019-0069-5, 2019.

Daellenbach, K. R., Bozzetti, C., Krepelova, A. K., Canonaco, F., Wolf, R., Zotter, P., Fermo, P., Crippa, M., Slowik, J. G., Sosedova, Y., Zhang, Y., Huang, R. J., Poulain, L., Szidat, S., Baltensperger, U., El Haddad, I., and Prevot, A. S. H.: Characterization and source apportionment of organic aerosol using offline aerosol mass spectrometry, Atmospheric Measurement Techniques, 9, 23-39, 10.5194/amt-9-23-2016, 2016.

Druge, T., Nabat, P., Mallet, M., Michou, M., Remy, S., and Dubovik, O.: Modeling radiative and climatic effects of brown carbon aerosols with the ARPEGE-Climat global climate model, Atmos. Chem. Phys., 22, 12167-12205, 10.5194/acp-22-12167-2022, 2022.

Du, Z., He, K., Cheng, Y., Duan, F., Ma, Y., Liu, J., Zhang, X., Zheng, M., and Weber, R.: A yearlong study of water-soluble organic carbon in Beijing II: Light absorption properties, Atmospheric Environment, 89, 235-241, http://dx.doi.org/10.1016/j.atmosenv.2014.02.022, 2014.

Finewax, Z., de Gouw, J. A., and Ziemann, P. J.: Identification and Quantification of 4-Nitrocatechol Formed from OH and NO_3 Radical-Initiated Reactions of Catechol in Air in the Presence of NO_x: Implications for Secondary Organic Aerosol Formation from Biomass Burning, Environ. Sci. Technol., 52, 1981-1989, 10.1021/acs.est.7b05864, 2018.

Gao, J., Wang, K., Wang, Y., Liu, S., Zhu, C., Hao, J., Liu, H., Hua, S., and Tian, H.: Temporal-spatial characteristics and source apportionment of $PM_{2.5}$ as well as its associated chemical species in the Beijing-Tianjin-Hebei region of China, Environ. Pollut., 233, 714-724, 10.1016/j.envpol.2017.10.123, 2018.

Ge, X., Li, L., Chen, Y., Chen, H., Wu, D., Wang, J., Xie, X., Ge, S., Ye, Z., Xu, J., and Chen, M.: Aerosol characteristics and sources in Yangzhou, China resolved by offline aerosol mass spectrometry and other techniques, Environ. Pollut., 225, 74-85, 10.1016/j.envpol.2017.03.044, 2017.

Gelencser, A., Hoffer, A., Kiss, G., Tombacz, E., Kurdi, R., and Bencze, L.: In-situ formation of light-absorbing organic matter in cloud water, Journal of Atmospheric Chemistry, 45, 25-33, 10.1023/a:1024060428172, 2003.

Gilardoni, S., Massoli, P., Paglione, M., Giulianelli, L., Carbone, C., Rinaldi, M., Decesari, S., Sandrini, S., Costabile, F., Gobbi, G. P., Pietrogrande, M. C., Visentin, M., Scotto, F., Fuzzi, S., and Facchini, M. C.: Direct observation of aqueous secondary organic aerosol from biomass-burning emissions, Proceedings of the National Academy of Sciences of the United States of America, 113, 10013-10018, 10.1073/pnas.1602212113, 2016.

Gligorovski, S., Strekowski, R., Barbati, S., and Vione, D.: Environmental Implications of Hydroxyl Radicals (•OH),

519   Chem. Rev., 115, 13051-13092, 10.1021/cr500310b, 2015.

520   Hammer, M. S., Martin, R. V., van Donkelaar, A., Buchard, V., Torres, O., Ridley, D. A., and Spurr, R. J. D.:
521   Interpreting the ultraviolet aerosol index observed with the OMI satellite instrument to understand absorption
522   by organic aerosols: implications for atmospheric oxidation and direct radiative effects, Atmos. Chem. Phys.,
523   16, 2507-2523, 10.5194/acp-16-2507-2016, 2016.

524   Heaton, T. H. E., Spiro, B., Madeline, S., and Robertson, C.: Potential canopy influences on the isotopic composition
525   of nitrogen and sulphur in atmospheric deposition, Oecologia, 109, 600-607, 10.1007/s004420050122, 1997.

526   Hodnebrog, O., Myhre, G., and Samset, B. H.: How shorter black carbon lifetime alters its climate effect, Nature
527   Communications, 5, 10.1038/ncomms6065, 2014.

528   Hsu, H.-I., Lin, M.-Y., Chen, Y.-C., Chen, W.-Y., Yoon, C., Chen, M.-R., and Tsai, P.-J.: An Integrated Approach to
529   Assess Exposure and Health-Risk from Polycyclic Aromatic Hydrocarbons (PAHs) in a Fastener
530   Manufacturing Industry, International Journal of Environmental Research and Public Health, 11, 9578-9594,
531   10.3390/ijerph110909578, 2014.

532   Hu, X., Belle, J. H., Meng, X., Wildani, A., Waller, L. A., Strickland, M. J., and Liu, Y.: Estimating
533        $PM_{2.5}$ Concentrations in the Conterminous United States Using the Random Forest Approach,
534   Environ. Sci. Technol., 51, 6936-6944, 10.1021/acs.est.7b01210, 2017.

535   Huang, R.-J., Yang, L., Cao, J., Chen, Y., Chen, Q., Li, Y., Duan, J., Zhu, C., Dai, W., Wang, K., Lin, C., Ni, H.,
536   Corbin, J. C., Wu, Y., Zhang, R., Tie, X., Hoffmann, T., O'Dowd, C., and Dusek, U.: Brown Carbon Aerosol in
537   Urban Xi'an, Northwest China: The Composition and Light Absorption Properties, Environ. Sci. Technol., 52,
538   6825-6833, 10.1021/acs.est.8b02386, 2018.

539   Jayne, J. T., Leard, D. C., Zhang, X. F., Davidovits, P., Smith, K. A., Kolb, C. E., and Worsnop, D. R.: Development
540   of an aerosol mass spectrometer for size and composition analysis of submicron particles, Aerosol Sci. Technol.,
541   33, 49-70, 10.1080/027868200410840, 2000.

542   Jo, D. S., Park, R. J., Lee, S., Kim, S.-W., and Zhang, X.: A global simulation of brown carbon: implications for
543   photochemistry and direct radiative effect, Atmos. Chem. Phys., 16, 3413-3432, 10.5194/acp-16-3413-2016,
544   2016.

545   Kampf, C. J., Jakob, R., and Hoffmann, T.: Identification and characterization of aging products in the
546   glyoxal/ammonium sulfate system - implications for light-absorbing material in atmospheric aerosols, Atmos.
547   Chem. Phys., 12, 6323-6333, 10.5194/acp-12-6323-2012, 2012.

548   Laskin, A., Laskin, J., and Nizkorodov, S. A.: Chemistry of Atmospheric Brown Carbon, Chem. Rev., 115, 4335-
549   4382, 10.1021/cr5006167, 2015.

550   Laskin, J., Laskin, A., Nizkorodov, S. A., Roach, P., Eckert, P., Gilles, M. K., Wang, B., Lee, H. J., and Hu, Q.:
551   Molecular Selectivity of Brown Carbon Chromophores, Environ. Sci. Technol., 48, 12047-12055,
552   10.1021/es503432r, 2014.

553   Lee, H. J., Aiona, P. K., Laskin, A., Laskin, J., and Nizkorodov, S. A.: Effect of Solar Radiation on the Optical
554   Properties and Molecular Composition of Laboratory Proxies of Atmospheric Brown Carbon, Environ. Sci.
555   Technol., 48, 10217-10226, 10.1021/es502515r, 2014.

556   Li, D., Wu, C., Zhang, S., Lei, Y., Lv, S., Du, W., Liu, S., Zhang, F., Liu, X., Liu, L., Meng, J., Wang, Y., Gao, J.,
557   and Wang, G.: Significant coal combustion contribution to water-soluble brown carbon during winter in Xingtai,
558   China: Optical properties and sources, J. Environ. Sci., 124, 892-900, 10.1016/j.jes.2022.02.026, 2023.

559   Li, J., Zhang, Q., Wang, G., Li, J., Wu, C., Liu, L., Wang, J., Jiang, W., Li, L., Ho, K. F., and Cao, J.: Optical
560   properties and molecular compositions of water-soluble and water-insoluble brown carbon (BrC) aerosols in
561   northwest China, Atmos. Chem. Phys., 20, 4889-4904, 10.5194/acp-20-4889-2020, 2020.

562   Li, L. J., Ho, S. S. H., Feng, B., Xu, H., Wang, T., Wu, R., Huang, W., Qu, L., Wang, Q., and Cao, J.: Characterization

of particulate-bound polycyclic aromatic compounds (PACs) and their oxidations in heavy polluted atmosphere: A case study in urban Beijing, China during haze events, Sci. Total Environ., 660, 1392-1402, 10.1016/j.scitotenv.2019.01.078, 2019a.

Li, X., Hu, M., Wang, Y., Xu, N., Fan, H., Zong, T., Wu, Z., Guo, S., Zhu, W., Chen, S., Dong, H., Zeng, L., Yu, X., and Tang, X.: Links between the optical properties and chemical compositions of brown carbon chromophores in different environments: Contributions and formation of functionalized aromatic compounds, Sci. Total Environ., 786, 10.1016/j.scitotenv.2021.147418, 2021a.

Li, Y., Ji, Y., Zhao, J., Wang, Y., Shi, Q., Peng, J., Wang, Y., Wang, C., Zhang, F., Wang, Y., Seinfeld, J. H., and Zhang, R.: Unexpected Oligomerization of Small alpha-Dicarbonyls for Secondary Organic Aerosol and Brown Carbon Formation, Environ. Sci. Technol., 55, 4430-4439, 10.1021/acs.est.0c08066, 2021b.

Li, Z., Nizkorodov, S. A., Chen, H., Lu, X., Yang, X., and Chen, J.: Nitrogen-containing secondary organic aerosol formation by acrolein reaction with ammonia/ammonium, Atmos. Chem. Phys., 19, 1343-1356, 10.5194/acp-19-1343-2019, 2019b.

Lin, G., Penner, J. E., Flanner, M. G., Sillman, S., Xu, L., and Zhou, C.: Radiative forcing of organic aerosol in the atmosphere and on snow: Effects of SOA and brown carbon, J. Geophys. Res.-Atmos., 119, 7453-7476, 10.1002/2013jd021186, 2014.

Lin, P., Liu, J., Shilling, J. E., Kathmann, S. M., Laskin, J., and Laskin, A.: Molecular characterization of brown carbon (BrC) chromophores in secondary organic aerosol generated from photo-oxidation of toluene, Physical Chemistry Chemical Physics, 17, 23312-23325, 10.1039/c5cp02563j, 2015.

Liu, D., He, C., Schwarz, J. P., and Wang, X.: Lifecycle of light-absorbing carbonaceous aerosols in the atmosphere, npj Clim. Atmos. Sci., 3, 40, 10.1038/s41612-020-00145-8, 2020a.

Liu, S., Huang, D., Wang, Y., Zhang, S., Liu, X., Wu, C., Du, W., and Wang, G.: Synergetic effects of NH3 and NOx on the production and optical absorption of secondary organic aerosol formation from toluene photooxidation, Atmos. Chem. Phys., 21, 17759-17773, 10.5194/acp-21-17759-2021, 2021.

Liu, S., Aiken, A. C., Gorkowski, K., Dubey, M. K., Cappa, C. D., Williams, L. R., Herndon, S. C., Massoli, P., Fortner, E. C., Chhabra, P. S., Brooks, W. A., Onasch, T. B., Jayne, J. T., Worsnop, D. R., China, S., Sharma, N., Mazzoleni, C., Xu, L., Ng, N. L., Liu, D., Allan, J. D., Lee, J. D., Fleming, Z. L., Mohr, C., Zotter, P., Szidat, S., and Prevot, A. S. H.: Enhanced light absorption by mixed source black and brown carbon particles in UK winter, Nature Communications, 6, 10.1038/ncomms9435, 2015.

Liu, X., Wang, H., Wang, F., Lv, S., Wu, C., Zhao, Y., Zhang, S., Liu, S., Xu, X., Lei, Y., and Wang, G.: Secondary Formation of Atmospheric Brown Carbon in China Haze: Implication for an Enhancing Role of Ammonia, Environ. Sci. Technol., 57, 11163-11172, 10.1021/acs.est.3c03948, 2023.

Liu, Y., Wang, T., Fang, X., Deng, Y., Cheng, H., Bacha, A.-U.-R., Nabi, I., and Zhang, L.: Brown carbon: An underlying driving force for rapid atmospheric sulfate formation and haze event, Sci. Total Environ., 734, 139415, 10.1016/j.scitotenv.2020.139415, 2020b.

Lu, J. W., Flores, J. M., Lavi, A., Abo-Riziq, A., and Rudich, Y.: Changes in the optical properties of benzo a pyrene-coated aerosols upon heterogeneous reactions with NO2 and NO3, Physical Chemistry Chemical Physics, 13, 6484-6492, 10.1039/c0cp02114h, 2011.

Lv, S., Wu, C., Wang, F., Liu, X., Zhang, S., Chen, Y., Zhang, F., Yang, Y., Wang, H., Huang, C., Fu, Q., Duan, Y., and Wang, G.: Nitrate-Enhanced Gas-to-Particle-Phase Partitioning of Water- Soluble Organic Compounds in Chinese Urban Atmosphere: Implications for Secondary Organic Aerosol Formation, Environmental Science & Technology Letters, 10, 14-20, 10.1021/acs.estlett.2c00894, 2023.

Meng, J., Wang, G., Li, J., Cheng, C., Ren, Y., Huang, Y., Cheng, Y., Cao, J., and Zhang, T.: Seasonal characteristics of oxalic acid and related SOA in the free troposphere of Mt. Hua, central China: Implications for sources and

formation mechanisms, Sci. Total Environ., 493, 1088-1097, 10.1016/j.scitotenv.2014.04.086, 2014.

Moise, T., Flores, J. M., and Rudich, Y.: Optical Properties of Secondary Organic Aerosols and Their Changes by Chemical Processes, Chem. Rev., 115, 4400-4439, 10.1021/cr5005259, 2015.

Nazarenko, L., Rind, D., Tsigaridis, K., Del Genio, A. D., Kelley, M., and Tausnev, N.: Interactive nature of climate change and aerosol forcing, J. Geophys. Res.-Atmos., 122, 3457-3480, 10.1002/2016jd025809, 2017.

Paatero, P. and Tapper, U.: Positive matrix factorization: A non-negative factor model with optimal utilization of error estimates of data values, Environmetrics, 5, 111-126, https://doi.org/10.1002/env.3170050203, 1994.

Qi, W. N., Zhang, Y. F., Shen, M. X., Li, L., Dai, W. T., Chen, Y. K., Liu, Y. L., Guo, X., Cao, Y., Wang, X., Jiang, Y. K., and Li, J. J.: Comparison of Gas-Particle Partitioning of Glyoxal and Methylglyoxal in the Summertime Atmosphere at the Foot and Top of Mount Hua, Molecules, 28, 10.3390/molecules28135276, 2023.

Qian, Y., Yasunari, T. J., Doherty, S. J., Flanner, M. G., Lau, W. K. M., Ming, J., Wang, H., Wang, M., Warren, S. G., and Zhang, R.: Light-absorbing Particles in Snow and Ice: Measurement and Modeling of Climatic and Hydrological impact, Adv. Atmos. Sci., 32, 64-91, 10.1007/s00376-014-0010-0, 2015.

Saleh, R., Marks, M., Heo, J., Adams, P. J., Donahue, N. M., and Robinson, A. L.: Contribution of brown carbon and lensing to the direct radiative effect of carbonaceous aerosols from biomass and biofuel burning emissions, J. Geophys. Res.-Atmos., 120, 10285-10296, 10.1002/2015jd023697, 2015.

Schnitzler, E. G., Gerrebos, N. G. A., Carter, T. S., Huang, Y., Healdc, C. L., Bertram, A. K., and Abbatt, J. P. D.: Rate of atmospheric brown carbon whitening governed by environmental conditions, Proceedings of the National Academy of Sciences of the United States of America, 119, 10.1073/pnas.2205610119, 2022.

Sumlin, B. J., Pandey, A., Walker, M. J., Pattison, R. S., Williams, B. J., and Chakrabarty, R. K.: Atmospheric Photooxidation Diminishes Light Absorption by Primary Brown Carbon Aerosol from Biomass Burning, Environmental Science & Technology Letters, 4, 540-545, 10.1021/acs.estlett.7b00393, 2017.

Sun, Y., Zhang, Q., Zheng, M., Ding, X., Edgerton, E. S., and Wang, X.: Characterization and Source Apportionment of Water-Soluble Organic Matter in Atmospheric Fine Particles (PM2.5) with High-Resolution Aerosol Mass Spectrometry and GC-MS, Environ. Sci. Technol., 45, 4854-4861, 10.1021/es200162h, 2011.

Sun, Y., Lei, L., Zhou, W., Chen, C., He, Y., Sun, J., Li, Z., Xu, W., Wang, Q., Ji, D., Fu, P., Wang, Z., and Worsnop, D. R.: A chemical cocktail during the COVID-19 outbreak in Beijing, China: Insights from six-year aerosol particle composition measurements during the Chinese New Year holiday, Sci. Total Environ., 742, 10.1016/j.scitotenv.2020.140739, 2020.

Van Damme, M., Clarisse, L., Whitburn, S., Hadji-Lazaro, J., Hurtmans, D., Clerbaux, C., and Coheur, P.-F.: Industrial and agricultural ammonia point sources exposed, Nat., 564, 99-103, 10.1038/s41586-018-0747-1, 2018.

Vione, D., Maurino, V., Minero, C., and Pelizzetti, E.: Aqueous atmospheric chemistry: Formation of 2,4-dinitrophenol upon nitration of 2-nitrophenol and 4-nitrophenol in solution, Environ. Sci. Technol., 39, 7921-7931, 10.1021/es050824m, 2005.

Vu, T. V., Shi, Z., Cheng, J., Zhang, Q., He, K., Wang, S., and Harrison, R. M.: Assessing the impact of clean air action on air quality trends in Beijing using a machine learning technique, Atmos. Chem. Phys., 19, 11303-11314, 10.5194/acp-19-11303-2019, 2019.

Wang, D., Shen, Z., Zhang, Q., Lei, Y., Zhang, T., Huang, S., Sun, J., Xu, H., and Cao, J.: Winter brown carbon over six of China's megacities: light absorption, molecularcharacterization, and improved source apportionment revealed by multilayerperceptron neural network, Atmos. Chem. Phys., 22, 14893-14904, 10.5194/acp-22-14893-2022, 2022a.

Wang, G., Li, J., Cheng, C., Hu, S., Xie, M., Gao, S., Zhou, B., Dai, W., Cao, J., and An, Z.: Observation of atmospheric aerosols at Mt. Hua and Mt. Tai in central and east China during spring 2009-Part 1: EC, OC and

651   inorganic ions, Atmos. Chem. Phys., 11, 4221-4235, 10.5194/acp-11-4221-2011, 2011.

652 Wang, G. H., Kawamura, K., Lee, S., Ho, K. F., and Cao, J. J.: Molecular, seasonal, and spatial distributions of
653   organic aerosols from fourteen Chinese cities, Environmental Science & Technology, 40, 4619-4625,
654   10.1021/es060291x, 2006.

655 Wang, G. H., Zhang, R. Y., Gomez, M. E., Yang, L. X., Zamora, M. L., Hu, M., Lin, Y., Peng, J. F., Guo, S., Meng,
656   J. J., Li, J. J., Cheng, C. L., Hu, T. F., Ren, Y. Q., Wang, Y. S., Gao, J., Cao, J. J., An, Z. S., Zhou, W. J., Li, G.
657   H., Wang, J. Y., Tian, P. F., Marrero-Ortiz, W., Secrest, J., Du, Z. F., Zheng, J., Shang, D. J., Zeng, L. M., Shao,
658   M., Wang, W. G., Huang, Y., Wang, Y., Zhu, Y. J., Li, Y. X., Hu, J. X., Pan, B., Cai, L., Cheng, Y. T., Ji, Y. M.,
659   Zhang, F., Rosenfeld, D., Liss, P. S., Duce, R. A., Kolb, C. E., and Molina, M. J.: Persistent sulfate formation
660   from London Fog to Chinese haze, Proceedings of the National Academy of Sciences of the United States of
661   America, 113, 13630-13635, 10.1073/pnas.1616540113, 2016.

662 Wang, Q., Zhou, Y., Ma, N., Zhu, Y., Zhao, X., Zhu, S., Tao, J., Hong, J., Wu, W., Cheng, Y., and Su, H.: Review of
663   Brown Carbon Aerosols in China: Pollution Level, Optical Properties, and Emissions, J. Geophys. Res.-Atmos.,
664   127, 10.1029/2021jd035473, 2022b.

665 Wang, S. and Li, H.: NO3 center dot-Initiated Gas-Phase Formation of Nitrated Phenolic Compounds in Polluted
666   Atmosphere, Environ. Sci. Technol., 55, 2899-2907, 10.1021/acs.est.0c08041, 2021.

667 Wu, C., Cao, C., Li, J., Lv, S., Li, J., Liu, X., Zhang, S., Liu, S., Zhang, F., Meng, J., and Wang, G.: Different
668   physicochemical behaviors of nitrate and ammonium duringtransport: a case study on Mt. Hua, China, Atmos.
669   Chem. Phys., 22, 15621-15635, 10.5194/acp-22-15621-2022, 2022.

670 Wu, C., Wang, G., Li, J., Li, J., Cao, C., Ge, S., Xie, Y., Chen, J., Li, X., Xue, G., Wang, X., Zhao, Z., and Cao, F.:
671   The characteristics of atmospheric brown carbon in Xi'an, inland China: sources, size distributions and optical
672   properties, Atmos. Chem. Phys., 20, 2017-2030, 10.5194/acp-20-2017-2020, 2020.

673 Wu, C., Observation of Brown carbon and its optical properties on Mt. Hua, Zenodo [data set],
674   https://doi.org/10.5281/zenodo.10926470, 2024.

675 Wu, C., Synchronous observation of aerosol at Mt. Hua, Version 1, Zenodo [data set],
676   https://doi.org/10.5281/zenodo.7413640, 2022a.

677 Yan, C., Zheng, M., Bosch, C., Andersson, A., Desyaterik, Y., Sullivan, A. P., Collett, J. L., Zhao, B., Wang, S., He,
678   K., and Gustafsson, O.: Important fossil source contribution to brown carbon in Beijing during winter, Sci. Rep.,
679   7, 10.1038/srep43182, 2017.

680 Yan, J., Wang, X., Gong, P., Wang, C., and Cong, Z.: Review of brown carbon aerosols: Recent progress and
681   perspectives, Sci. Total Environ., 634, 1475-1485, 10.1016/j.scitotenv.2018.04.083, 2018.

682 Zhang, A., Wang, Y., Zhang, Y., Weber, R. J., Song, Y., Ke, Z., and Zou, Y.: Modeling the global radiative effect of
683   brown carbon: a potentially larger heating source in the tropical free troposphere than black carbon, Atmos.
684   Chem. Phys., 20, 1901-1920, 10.5194/acp-20-1901-2020, 2020.

685 Zhang, Y., Forrister, H., Liu, J., Dibb, J., Anderson, B., Schwarz, J. P., Perring, A. E., Jimenez, J. L., Campuzano-
686   Jost, P., Wang, Y., Nenes, A., and Weber, R. J.: Top-of-atmosphere radiative forcing affected by brown carbon
687   in the upper troposphere, Nat. Geosci., 10, 486-489, 10.1038/ngeo2960, 2017.

688 Zhao, R., Lee, A. K. Y., Huang, L., Li, X., Yang, F., and Abbatt, J. P. D.: Photochemical processing of aqueous
689   atmospheric brown carbon, Atmos. Chem. Phys., 15, 6087-6100, 10.5194/acp-15-6087-2015, 2015.

690

691
692
693
694
695
696

Table 1 Optical properties of BrC and mass concentrations organic carbon/nitrogen in $PM_{2.5}$ and meteorological parameters at the two sampling sites.

699

	Mountain foot (MF)			Mountainside (MS)		
	Average	Daytime	Nighttime	Average	Daytime	Nighttime
(i) Optical properties of BrC and acidity of $PM_{2.5}$						
abs_{365} (M m^{-1})	5.1±2.4	5.0±2.5	5.2±2.2	2.1±1.4	2.6±1.3	1.6±1.3
MAE_{365} (m^2 g^{-1})	0.69±0.2	0.66±0.18	0.73±0.18	0.67±0.21	0.67±0.15	0.68±0.26
AAE	6.0±0.5	6.1±0.51	6.0±0.51	5.7±1.3	5.5±0.9	5.8±1.7
abs_{365}-BrC/abs_{550}-BC[a]	0.18±0.09	0.22±0.08	0.17±0.09	0.26±0.08	0.28±0.08	0.25±0.07
pH	2.9±2.0	2.3±1.6	3.6±2.1	3.4±2.2	3.5±2.2	3.3±2.2
(ii) Concentrations of carbonaceous $PM_{2.5}$ and aerosol liquid water content (ALWC)						
WSOC (µgC m^{-3})	7.3±2.5	7.6±2.8	7.0±2.1	3.2±2.1	4.0±2.1	2.4±1.7
WSON (µgN m^{-3})	2.3±1.6	2.5±1.7	2.0±1.4	1.2±0.9	1.5±1.1	0.8±0.7
OC (µgC m^{-3})	14.0±4.7	12.4±4.6	15.4±4.4	5.0±2.8	6.3±2.8	3.8±2.3
EC (µgC m^{-3})	4.3±2.0	3.1±1.0	5.4±1.9	1.1±0.7	1.3±0.7	0.8±0.4
Nitrophenols (ng m^{-3})	16±13	12±10	19±15	2.5±1.9	3.2±2.2	1.7±1.1
ALWC (µg m^{-3})	28±64	11±15	44±86	27±71	18±24	35±95
WSOC/OC	0.54±0.15	0.62±0.13	0.47±0.11	0.62±0.21	0.62±0.16	0.61±0.25
(iii) Meteorological parameters						
T (℃)	23±4.2	27±3.0	20±2.4	15±2.5	16±2.3	14±2.3
RH (%)	69±18	56±14	81±14	63±20	62±19	63±21
Wind speed (m s^{-1})	1.3±1.1	1.5±0.93	1.2±1.2	3.2±2.0	2.7±1.5	3.8±2.3
Visibility (km)	14±9.5	16±9.6	12±9.0	22±12.1	21±12	24±12.0

[a]The $abs_{550\text{-}BC}$ was calculated according to the mass absorption efficiency (MAE) of BC (black carbon) reported by Bosch et al. (2014), and the light wavelengths for the abs_{365}-BrC and abs_{550}-BC are 365 nm and 550 nm, respectively.

703

704
705

706
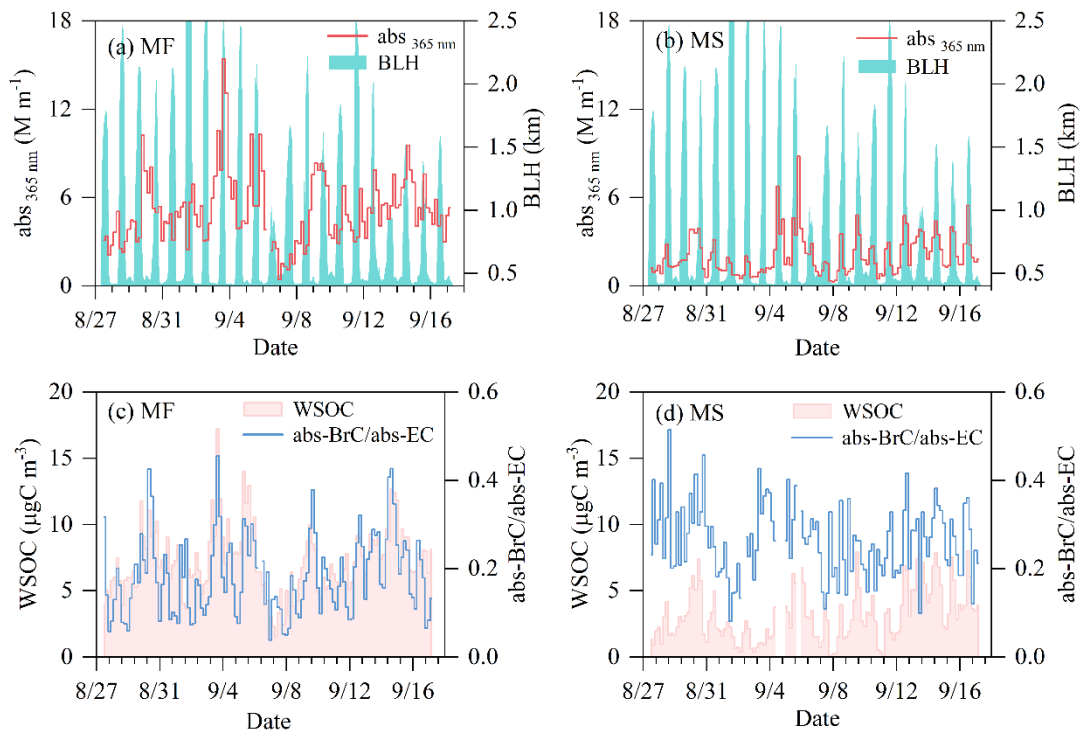
707 **Figure 1. Temporal variations of light absorption of BrC in the ground surface (mountain**
708 **foot site, MF) and the upper boundary layer (mountainside site, MS) atmospheres in**
709 **inland China**. (a, b) Abs_{365} and boundary layer height (BLH). (c, d) Concentration of WSOC
710 and the ratio of light absorption of BrC at λ=365 nm to BC at λ= 550 nm.

711
712

713

714

715
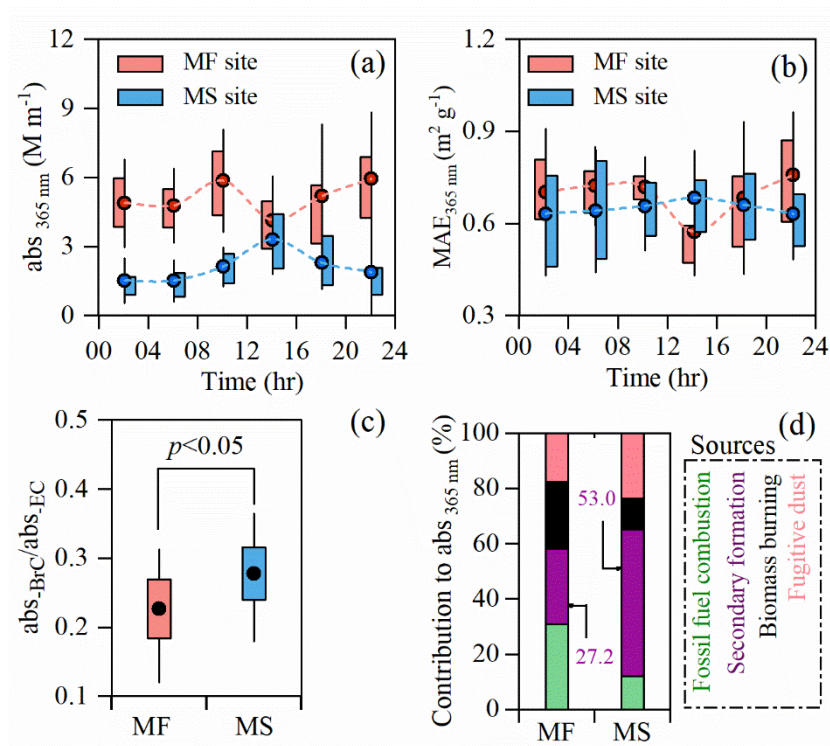
Figure 2. BrC formation in air mass lifting process. (a) and (b) Diurnal variations in abs_{365nm} and MAE at the mountain foot (MF) and mountainside (MS) sites. (c) Ratio of light absorption of BrC at $\lambda=365$ nm to that of BC (abs_{-BrC}/abs_{-BC}) at $\lambda=550$ nm in daytime at both sites (The abs_{-BC} at $\lambda=550$ nm was calculated according to mass absorption efficiency of EC reported by Bosch et al. (2014). (d) Source apportionment for the daytime BrC at the two sites. The whisker boxes show mean (dot), 25th–75th percentile ranges (box), and standard deviation values (whiskers).

723
724
725
726
727
728

729

730 **Figure 3. Evolution in chemical composition of daytime water-soluble BrC in the air mass**
731 **transport from the mountain foot (MF site, red dots) to the mountainside (MS site, blue**
732 **dots).** (a) and (c) Light absorption (abs$_{365}$) of daytime water-soluble BrC as a function of their
733 oxidation state (OSc=2O/C−H/C) at MF and MS sites, respectively. (b) The VK-triangle
734 diagram of water-soluble BrC at the two sites.
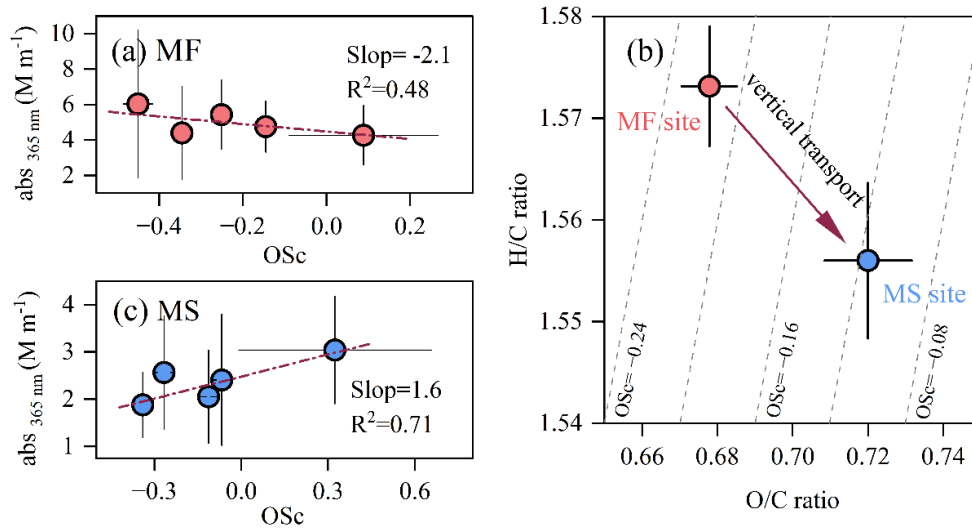
735
736
737
738
739
740
741
742
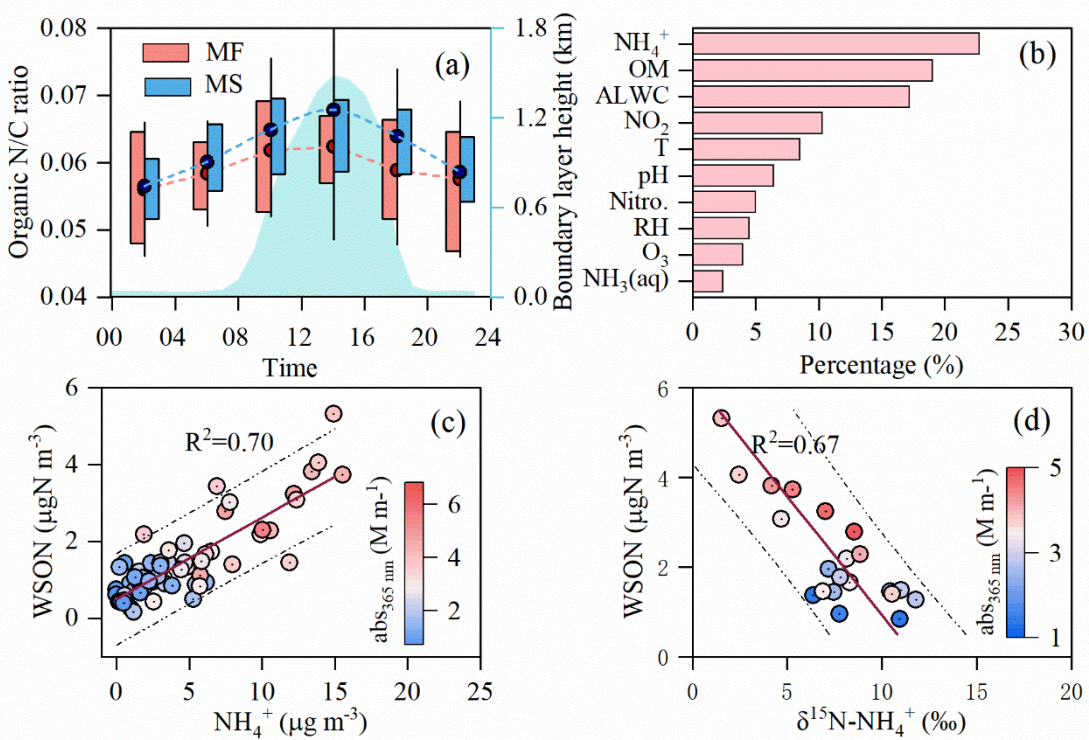
Figure 4. **Formation of water-soluble organic nitrogen compounds (WSONs) in the air mass lifting process.** (a) Diurnal variations in elemental ratio of N/C of fine particulate water-soluble organics at the mountain foot (MF) and mountainside (MS) sites, the whisker boxes show mean (dot), 25th–75th percentile ranges (box), and standard deviation values (whiskers). (b) Importance assessment for the key factors affecting the daytime WSON at MS site. (c) and (d) Linear fit regressions for WSONs with NH_4^+ and $\delta^{15}N\text{-}NH_4^+$ in the daytime $PM_{2.5}$ aerosols at MS site, respectively.

753

754
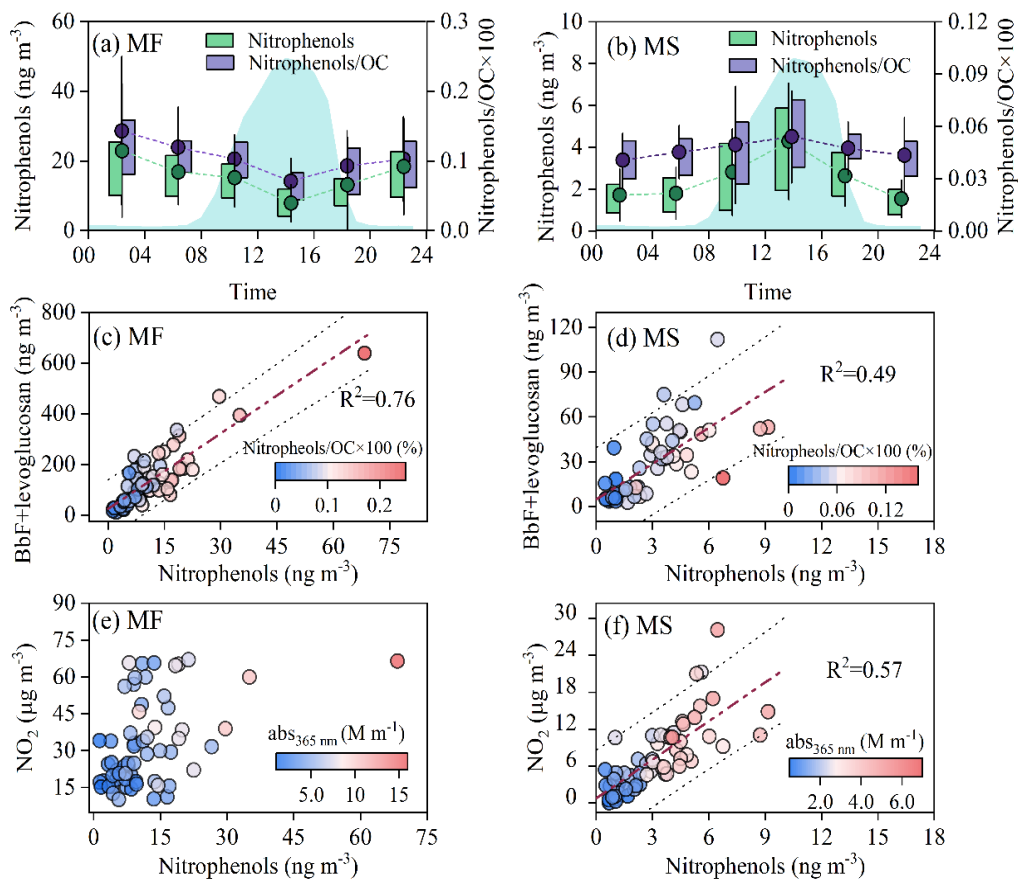
Figure 5. The source and secondary formation for nitrophenols at MF and MS sites. (a and b)
Diurnal variations in nitrophenols and mass ratio of nitrophenols to OC (nitrophenols/OC); blue
sky shade indicates diurnal variation of boundary layer height, and the whisker boxes show
mean (dot), 25th–75th percentile ranges (box), and standard deviation values (whiskers). Linear
fit regression for nitrophenols with BbF+levoglucosan (c and d) and NO_2 (e and f),
respectively.

762

763
764
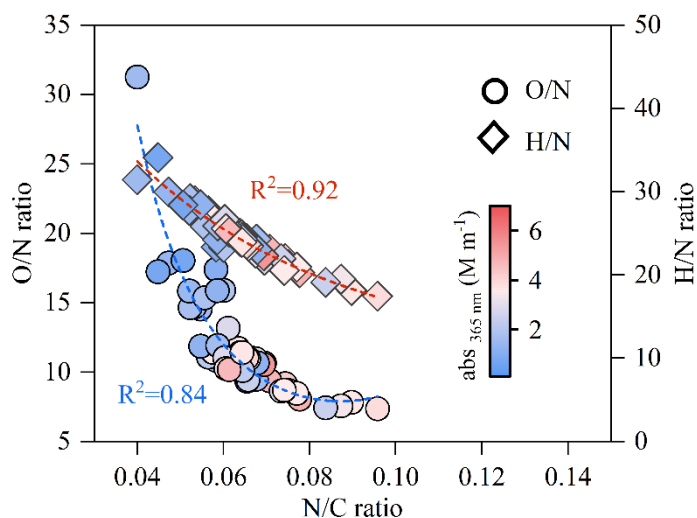
765
766 **Figure 6.** Elemental composition of daytime WSOC at MS site.

767
768
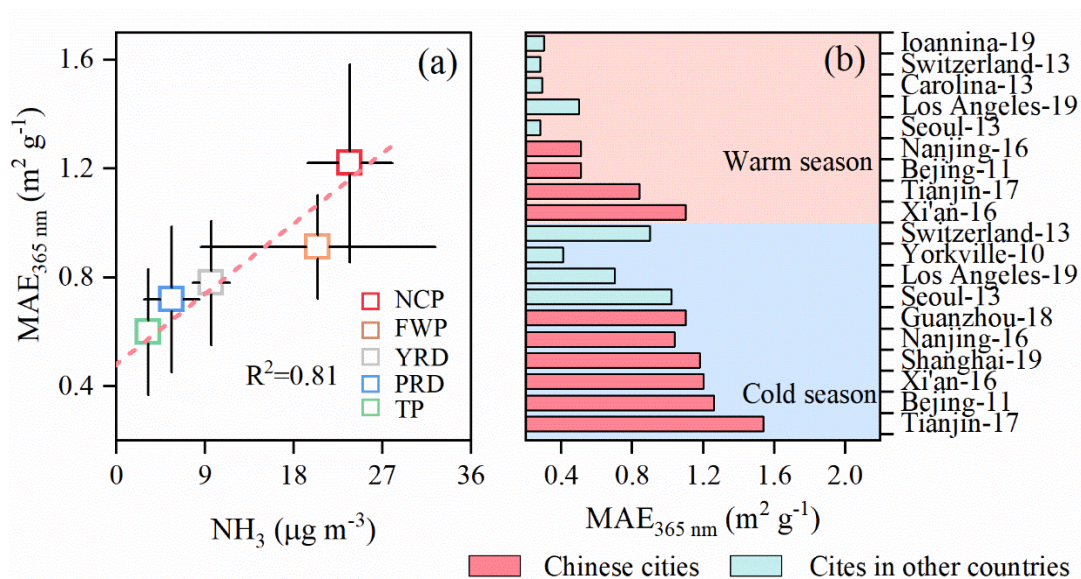
769
770 **Figure 7. Impact of NH₃ on atmospheric BrC over China**. (a) Linear correlation between
771 NH$_3$ and MAE of BrC in different regions of China (NCP, north China Plain; FWP: Fenwei
772 Plain; YRD, Yangtze River delta; PRD, Pearl River delta; TP: Tibetan Plain). (b) MAE$_{365}$ of
773 BrC in China and other countries (The details of datasets from literatures, including specific
774 sites, time periods, and sources, etc., are given in Table S4 and S5).
775